Materials Today Communications 25 (2020) 101607

Contents lists available at ScienceDirect

Materials Today Communications

journal homepage: www.elsevier.com/locate/mtcomm

Artifact-free bulk nanocrystalline Al-Li alloys with multiple deformation mechanisms and improved tensile properties

Sara I. Ahmad [a], Leena A. Al-Sulaiti [b], K. Andre Mkhoyan [c], Khaled M. Youssef [d,*]

[a] Department of Sustainable Development, Hamad Bin Khalifa University, Doha 5825, Qatar
[b] Department of Mathematics, Statistics, and Physics, Qatar University, Doha 2713, Qatar
[c] Department of Chemical Engineering and Materials Science, University of Minnesota, Minneapolis 55455, MN, USA
[d] Materials Science and Technology-Master Program, Qatar University, Doha 2713, Qatar

ARTICLE INFO

Keywords:
Nanocrystalline materials
Aluminum
Lithium
Mechanical properties
Twinning

ABSTRACT

An artifact-free bulk nanocrystalline (NC) aluminum (Al)-2% lithium (Li) alloy was synthesized in this study using *in-situ* consolidation via a combination of cryogenic and room temperature milling. The mechanical behavior of this alloy was investigated by tensile testing and microhardness measurements, and it was compared with coarse-grained (CG) Al alloys and a commercially pure NC Al synthesized using the same method. The transmission electron microscopy (TEM) analysis revealed that the grain size of the NC Al-2% Li alloy and NC pure Al are 18 nm and 29 nm, respectively. The NC Al-Li alloy showed extremely high yield and ultimate tensile strength values of 440 MPa and 556 MPa, respectively. In addition, a high tensile ductility of 14% was achieved in the NC Al-Li alloy along with a relatively high strain hardening exponent (0.11). The high-resolution TEM investigations indicate a dependency of these extraordinarily tensile properties on multiple deformation mechanisms such as dislocation slip and pile-up and deformation twinning.

1. Introduction

Increasing demands for superior fuel consumption and lower greenhouse gas emissions has driven the interests to design new high-performance and lightweight structural materials [1]. In this regard, aluminum (Al) alloys are known to possess promising high specific strengths, amongst other attractive properties, such as corrosion resistance, the capability to be strengthened by precipitation or second phases, along with its versatility to be shaped and machined [2]. Thus, Al alloys are promising candidates for improving energy efficiency in fuel-consumption applications that require lightweight and high-strength materials [1,2]. Lithium (Li) is the lightest metal to exist, and it is one of only a few metals that possesses moderate solubility in Al [2,3]. Reportedly, alloying Al with 1% Li decreases its density by 3% and increases its elastic modulus by 6% [2,3]. Extensive research has been carried out worldwide on lithium-containing aluminum alloys in weight-critical and stiffness-critical structures for military, space and commercial applications because they offer the promise of low density, improved specific strength and high stiffness-to-weight ratio over the other commercial 2XXX and 7XXX series aluminum alloys and carbon-fiber composites [4–6]. However, these alloys were designed for the best performance in their coarse-grained state. It is long overdue to design aluminum-lithium based alloys for the best performance in their nanostructured state.

There have been continuous research efforts to produce such alloys with grain sizes in the nanoscale range (< 100 nm) in order to further improve their mechanical properties. The strength and hardness of these nanocrystalline (NC) metals and alloys have been reported to be at least an order of magnitude higher than their coarse-grained (CG) counterparts. However, most of these materials showed a lack of strain hardening and exhibited poor ductility due to plastic instability in tension [7–11]. This behavior had been reported for the majority of metals, including NC Al and Al alloys [12–14]. Liu et al. [12] reported a high yield strength of 260 MPa but with a low 3.1% total elongation for their nanosized Al powder (80 nm) that was consolidated by a spark plasma sintering technique (SPS). A significantly high 500 MPa tensile yield strength was reported by Choi et al. [13] for NC Al (48 nm); this was associated with early plastic failure and a total elongation of 2%. Similarly, high tensile yield strength of 641 MPa was reported by Witkin et al. [14] for NC Al-7.5% Mg (20 nm) but with a limited 5.4% ductility. This limited ductility is a significant concern for the applications of these novel materials.

* Corresponding author.
E-mail address: kyoussef@qu.edu.qa (K.M. Youssef).

https://doi.org/10.1016/j.mtcomm.2020.101607
Received 23 April 2020; Received in revised form 21 August 2020; Accepted 21 August 2020
Available online 31 August 2020

Additionally, recent studies on the deformation behavior of NC Al reported the activation of unconventional plastic deformation by twinning. It is well known that CG Al possesses a high stacking fault energy that restricts its deformation by twinning [15,16]. However, molecular dynamic simulations (MDS) predicted the formation of deformation twins in NC Al [17–19]. Experimentally, twinning has been observed in ball-milled NC Al [20,21] and in NC Al films produced by physical vapor deposition and deformed by micro indentation [22]. It is believed that the distinct structural features of the nanostructure, along with the associated extremely high strength, could trigger unique plastic deformation mechanisms that otherwise cannot be observed in CG Al [22–26]. There is a lack of reports about the influence of these unconventional deformation mechanisms on the overall tensile properties of NC Al-Li alloys. Therefore, we report in this paper an investigation of the mechanical properties and the associated deformation behavior in designed, artifact-free bulk NC Al–2% Li alloys, which is synthesized through *in-situ* consolidation during mechanical alloying. The mechanical behavior of the produced alloy is evaluated through tensile tests and microhardness. The nanostructure and deformation mechanisms are examined using TEM.

2. Experimental procedure

A sample with a bulk composition of Al-2% Li (weight %) was prepared from pure Al powder (99.99%, -325 mesh, from Alfa Aesar) and pure Li granules (99%, from Alfa Aesar). The ball milling of the Al-2% Li sample was conducted using an SPEX 8000 shaker mill. The Al powder and the Li granules were loaded into a stainless steel vial along with stainless steel balls using a ball-to-powder ratio of 10:1. The total weight of the powder for each run was 3 g. The loading and sealing of the sample were done in a glovebox under ultra-high purity argon (oxygen level < 0.5 ppm) to eliminate the oxidation during milling. The synthesis of the artifact-free bulk NC Al-2% Li alloy was then conducted in two stages. During the first stage of milling, a specially-designed Teflon vial was used to hold the stainless steel vial. Liquid nitrogen (LN) was allowed to flow around the stainless steel vial to maintain the temperature at about 77 K. To prevent nitrogen and oxygen contamination and to secure the sealing of the stainless steel vial at low temperatures during cryogenic milling, a custom-designed PFA Teflon O-ring encapsulating a 302 stainless steel wound ribbon spring (NESAstra Seals) was used. The second stage of milling was conducted at room temperature without using the Teflon vial. No process control agents were used during both stages of the ball milling. For comparison, a pure NC Al sample was prepared using the same method.

The uniformity of the *in-situ* consolidation of the bulk spheres was investigated. The bulk spheres were sliced using a diamond saw, and the microhardness was measured across the cross-sectional area of the sliced spheres. A Future Tech Microhardness Tester, FM-800, equipped with a fully automated hardness testing system (ARS9000), was used for hardness measurements. The microhardness indentation parameters included a 25 g load and a dwelling time of 10 s with at least eight indentations per sample. The density of the *in-situ* consolidated samples was measured using the Sartorius density determination kit (Sartorius YDK03, Germany). The density determination kit was set up using distilled water, and the water's temperature was monitored during the measurement. Five density measurements were carried out for each sample.

To investigate the nanostructure of the *in-situ* consolidated bulk alloy, an FEI Tecnai G2 transmission electron microscope (TEM) operated at 200 kV was used. The TEM samples were prepared using a twin jet electropolishing device (Fischione Model 110) along with an electrolytic bath of 10 % perchloric acid and 90 % ethyl alcohol at ~ 233 K. For tensile testing, the *in-situ* consolidated spheres were compacted in an 8 mm diameter tungsten carbide die. Several thin disks were cut from the compacted cylinders using a diamond saw, which were later cut into dog-bone shaped tensile specimens with a gauge length of 3 mm and a width of 1 mm. The final thicknesses of the tensile samples ranged between 250 and 370 μm after polishing the surfaces of the samples to a mirror finish. The tensile tests were performed using a miniaturized tensile machine (eXpert 4200 series, from ADMET Inc.) with a strain rate of 10^{-3} s^{-1} at room temperature. The strain during tensile tests was measured using a 3-mm gauge length extensometer (from Epsilon Technology Corp.), and the tensile machine was calibrated for the compliance errors. The fracture surface of the tensile samples was studied using an FEI Nova NanoSEM—scanning electron microscope (SEM).

3. Results and discussion

3.1. Evolution of the nanostructure

The *in-situ* consolidated NC Al-2% Li spheres were synthesized in this work using a combination of liquid nitrogen and room temperature ball milling. For comparison, the same technique and conditions were used to synthesize pure NC Al. The final *in-situ* consolidated bulk spheres of NC Al-2% Li and NC Al are shown in Fig. 1, and they exhibit diameters up to 10 mm and 6 mm, respectively. Utilizing the cryogenic and the subsequent room temperature ball milling techniques allowed for tailoring the samples from fine powders into bulk spheres. Initially, milling at cryogenic temperatures for 2 h suppressed the dynamic recovery of dislocations and allowed for higher dislocation densities, which resulted in grain refinement. It is crucial for a successful *in-situ* consolidation process to keep the vial completely immersed in LN by applying a continuous high liquid nitrogen flow. If the flow rate of LN is relatively low or interrupted during cryogenic milling, flake-shaped pieces are typically formed (see Fig. 1A), and further room temperature milling would produce hollow spheres. However, keeping the temperature of the powder and milling media as low as possible by increasing the flow rate of LN facilitates the formation of small spherical agglomerates (see Fig. 1A). The heat generated during the room temperature ball milling for 4 h favors the consolidation of the spherical agglomerates into artifact-free bulk spheres (see Fig. 1B and C).

To investigate the integrity of the consolidated structure and the uniformity of the microstructure, the NC Al-2% Li and NC Al spheres were sliced across their diameters. The spheres appear to be fully densified with no observed porosities or voids (see Fig. 1C). The sliced spheres were then mechanically polished, and their microhardness values were evaluated using Vickers microhardness across the diameter (see Fig. 2). Uniform microhardness values were obtained across the diameters of the polished surfaces for both NC Al-2% Li and NC Al samples, with their average hardness values being 1.44 GPa and 1.1 GPa, respectively. The uniform microhardness values across the spheres indicate the homogeneity of the microstructure and thus the applicability of the *in-situ* consolidation technique. The microhardness value of the Al-2% Li alloys is higher than that of the Al-2Li alloys produced by accumulative roll bonding and aging treatment (~60 HV) [27] and the Al-2.3 % Li alloys processed using solution treatment and rolling with the cyclic movement of rolls technique (1.2 HV) [28].

Fig. 3A and B are typical bright-field TEM (BF-TEM) images of the *in-situ* consolidated NC Al-2% Li and NC Al spheres after combined milling of 6 h. The grains in both samples appear to be equiaxed with random orientations, and they are separated by high-angle grain boundaries [29]. Fig. 4A and B present the grain size distribution of NC Al-2% Li and NC Al, respectively. The statistical analysis was performed on 250 grains for each sample and showed a monotonic grain size distribution with an average grain size of 18 nm and 29 nm for NC Al-2% Li and Al, respectively. The selected area diffraction patterns for the NC Al-2% Li and Al are shown in the inset images in Fig. 3A and B, respectively, and they illustrate the presence of only the face-centered cubic (FCC) Al phase. The absence of any Li body-centered cubic (BCC) rings in the Al-2% Li diffraction pattern is an indication of complete solubility of Li in Al and the formation of an FCC supersaturated solid solution. The

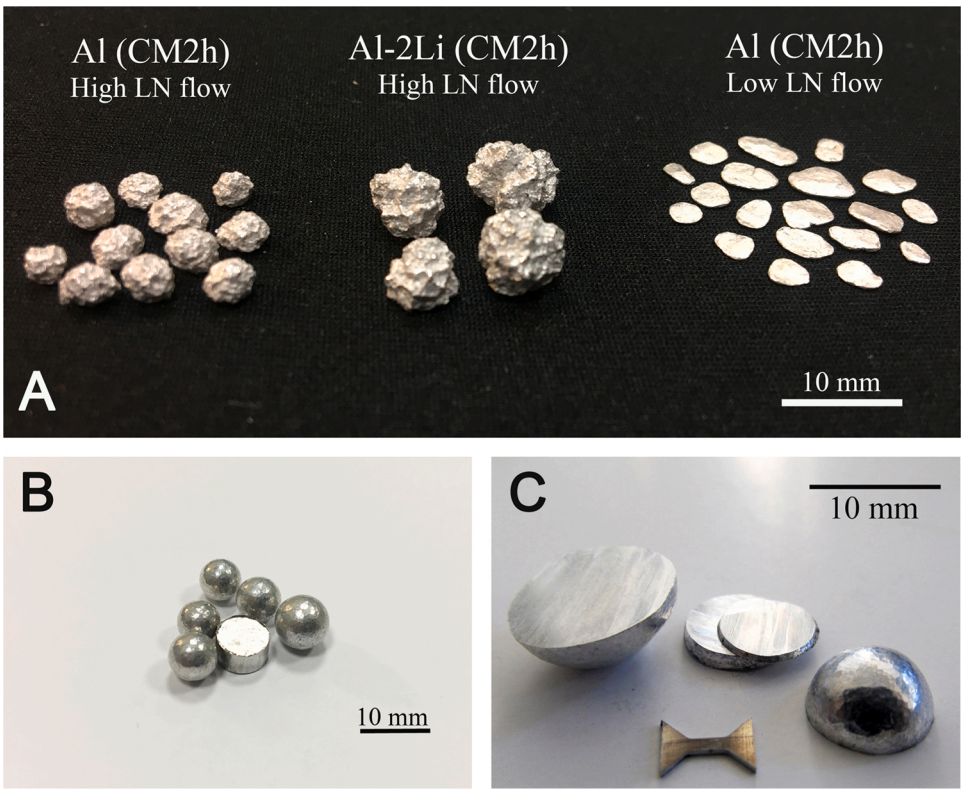

Fig. 1. (A) The effect of the liquid nitrogen flow on the shape of the Al agglomeration after 2 h of cryogenic milling, (B) and (C) are the *in-situ* consolidated final spheres of the NC Al and Al-2% Li, respectively, after 6 h of combined cryogenic and room temperature milling.

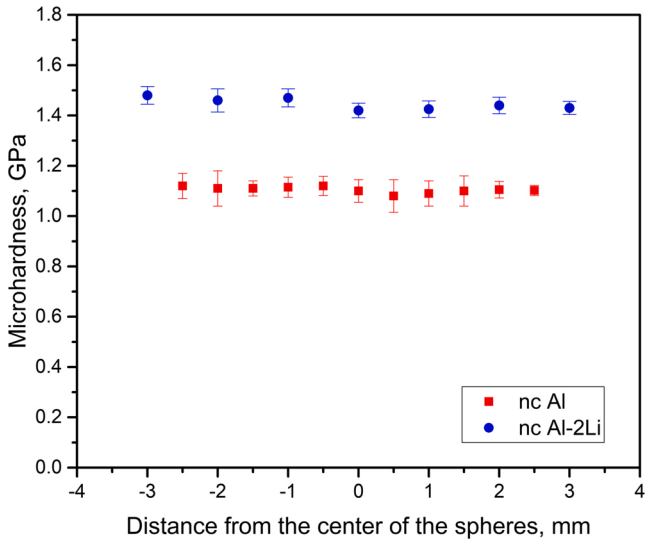

Fig. 2. Vickers microhardness variation across the diameter of the *in-situ* consolidated NC Al and Al-2% Li spheres.

formation of solid solutions during mechanical milling has been reported for various systems [8,30]. The severe plastic deformation during milling increases the solid solubility limit of miscible systems and even produces alloys from immiscible elements, which otherwise do not attain an equilibrium room temperature solubility. This is attributed to the large grain boundary density and, thus, the large number of segregation sites produced during mechanical milling as a result of the severe plastic deformation [31]. For instance, Youssef et al. [8] reported the formation of a supersaturated Al-4.5% Mg alloy using *in-situ* consolidation mechanical milling, thus increasing the maximum solid solubility of Mg in Al from 1%. In the case of immiscible systems, Botcharova et al. [30] reported the alloying of 10 % Nb in Cu using mechanical milling.

The BF-TEM image of the *in-situ* consolidated NC Al revealed the presence of deformation twins (see red arrows in Fig. 3B). A closer investigation using high-resolution TEM (HR-TEM) confirmed the presence of deformation twins distributed in both the NC Al-2% Li and Al samples. These twins are identified as planer defects with parallel boundaries and can be recognized by the mirror symmetry between the twin and the parent lattice (see Fig. 5A and B). They seemed to mostly form in relatively small nanograins and emitted from the grain boundaries on {111} slip planes, along with stacking faults, which could facilitate the creation of these deformation twins. A statistical analysis relating the number and size of grains containing deformation twins in both NC Al-2% Li and Al samples was performed on 40 NC Al-2% Li grains and NC Al grains (see Fig. 3A and B), respectively. It was observed that the majority of deformation twins in both samples resided in relatively small grains with grain size values ranging between 10 and 25 nm. It is well known that the high stacking fault energy in CG Al has long prevented its deformation by twinning [15,16]. Recently, Zhao et al. [32] were able to induce macro-deformation twins in single-crystal Al by providing ultrahigh strain rates ($\sim 10^6\ s^{-1}$) and high shear strain (200%) using a dynamic equal channel angular pressing technique. Recent studies have shown that deformation by twinning is made possible in NC Al [20–22]. The high resolution TEM investigations by Chen et al. [22] on the NC Al films, which were deformed by microindentations and manual grinding, revealed the presence of deformation twins in relatively smaller grains, consistent with our observations. They calculated the shear stresses required to activate a partial and a full lattice dislocation in Al as a function of grain size using the classical dislocation theory [22]. It was also found that as the grain size decreases gradually below about 10 nm, the shear stress needed to form a partial dislocation becomes smaller than the stress needed to form a full dislocation. Thus, the emission of a partial dislocation in Al becomes easier than that of the lattice dislocation, which facilitates the formation of twins in the small

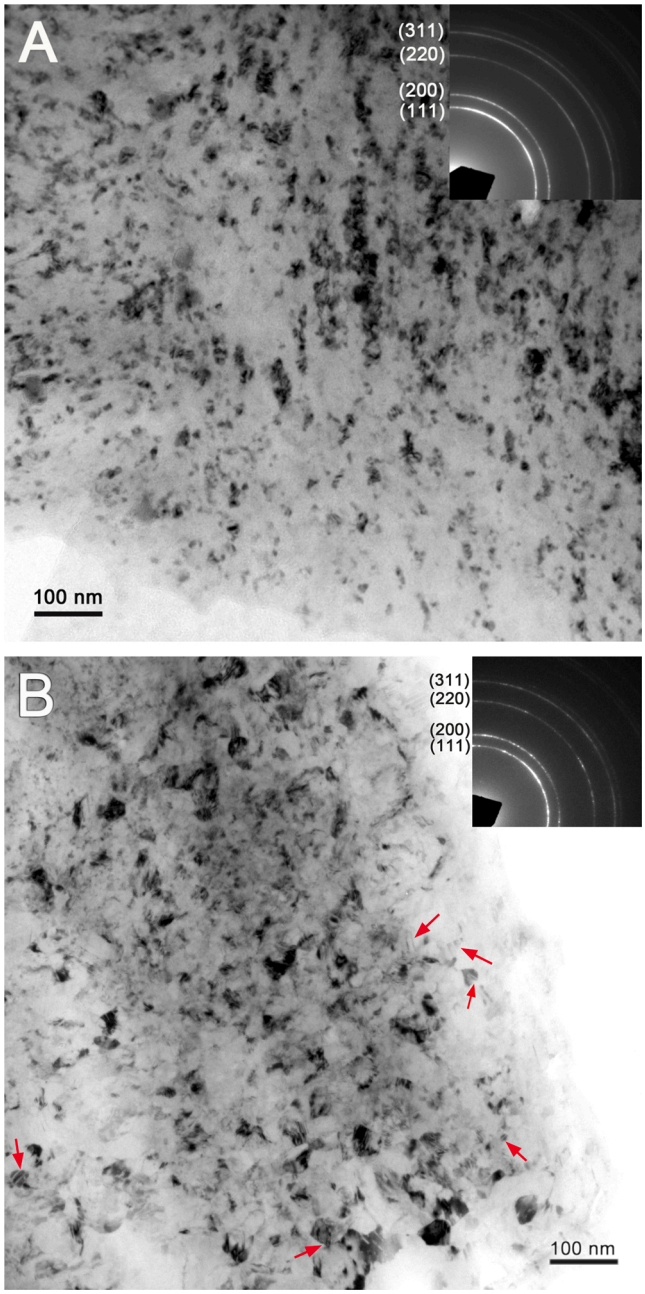

Fig. 3. BF-TEM micrographs after combined milling showing nanocrystalline grains of (A) NC Al-2% Li, and (B) NC Al. Inset images in (A) and (B) show the indexed selected area electron diffraction patterns of the NC Al-2% Li and NC Al samples, respectively. Red arrows in (B) point to the deformation twins distributed in the NC Al sample. (For interpretation of the references to color in this figure legend, the reader is referred to the web version of this article.)

nanoscale grains. Liao et al. [21] studied the formation mechanisms of deformation twins as they reported two types of twins via TEM observations in their NC Al synthesized by ball milling while immersing the Al powder in liquid nitrogen. They were able to verify different twinning formation mechanisms and confirm the twinning mechanisms predicted by the molecular dynamic simulation (MDS) [18], including the heterogeneous nucleation and growth of twins from grain boundaries and the twin lamella formation by the dissociation and migration of grain boundaries. These reports and our observations are in agreement with the MDS by Yamakov et al. [17,18] and the analytical model by Zhu et al. [33], which relates the grain size of NC FCC Al to its deformation by twinning. These findings suggest that twinning, although a

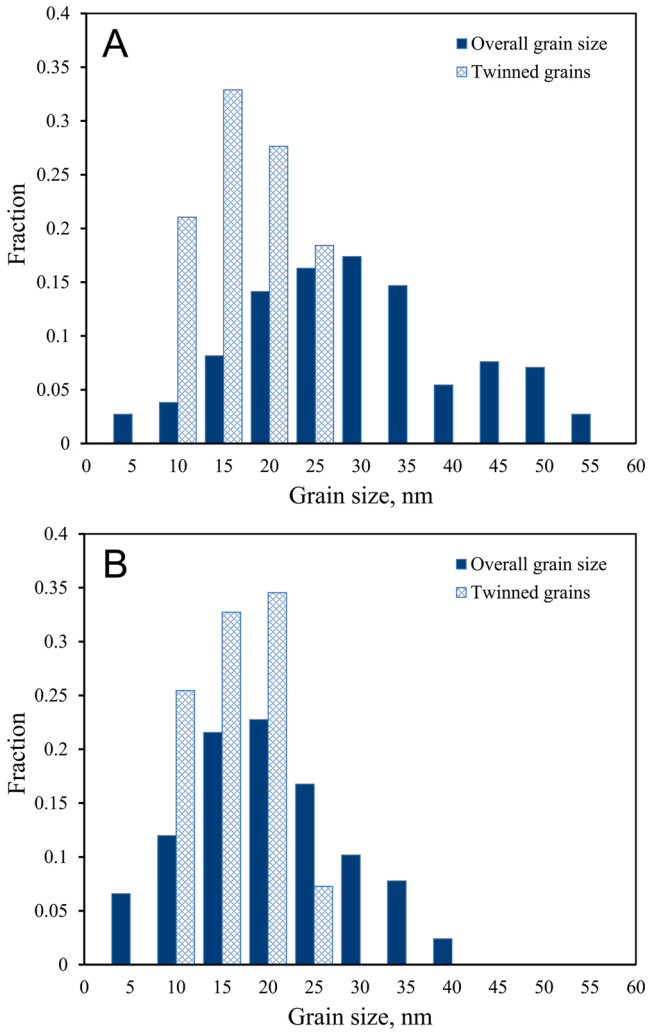

Fig. 4. Statistical grain size distribution of all grains and the twins-containing grains of (A) NC Al-2% Li, and (B) NC Al.

non-favorable deformation mechanism in conventional grain-size Al because of the high stacking fault energy, is a preferred mechanism of deformation in the NC Al and Al-2% Li alloy. In addition, Muzyk et al. [34] used a density function theory to calculate the generalized stacking fault energy of Al alloys. Lithium was found to be one of the alloying elements that reduced the stacking fault energy of Al and promoted the emission of partial dislocations, which in turn facilitate the formation of twins. In FCC metals, different twinning formation mechanisms have been reported [20,21,32,33,35–37]. In our *in-situ* consolidated NC Al-2% Li, it appears that the emission of partial dislocations from the grain boundaries on {111} slip planes could be the main reason for the formation of the observed twins, see Fig. 5A.

3.2. Mechanical properties

The tensile tests were conducted to investigate the mechanical behavior of the *in-situ* consolidated NC Al-2% Li sample. For comparison purposes, similar tensile tests were conducted on the NC Al sample and a commercially pure CG Al sheet (from Alfa Aesar, 99% purity). Fig. 6A shows the tensile stress-strain curves obtained for the NC Al-2% Li, NC Al, and CG commercially pure Al samples. The resulting tensile properties of the three samples are summarized in Table 1. In comparison to the CG commercially pure Al, both the *in-situ* consolidated NC Al and Al-2% Li showed lower elongation to failure levels but significantly higher yield strengths (σ_y at 0.2% offset) and ultimate tensile strengths (σ_u). The

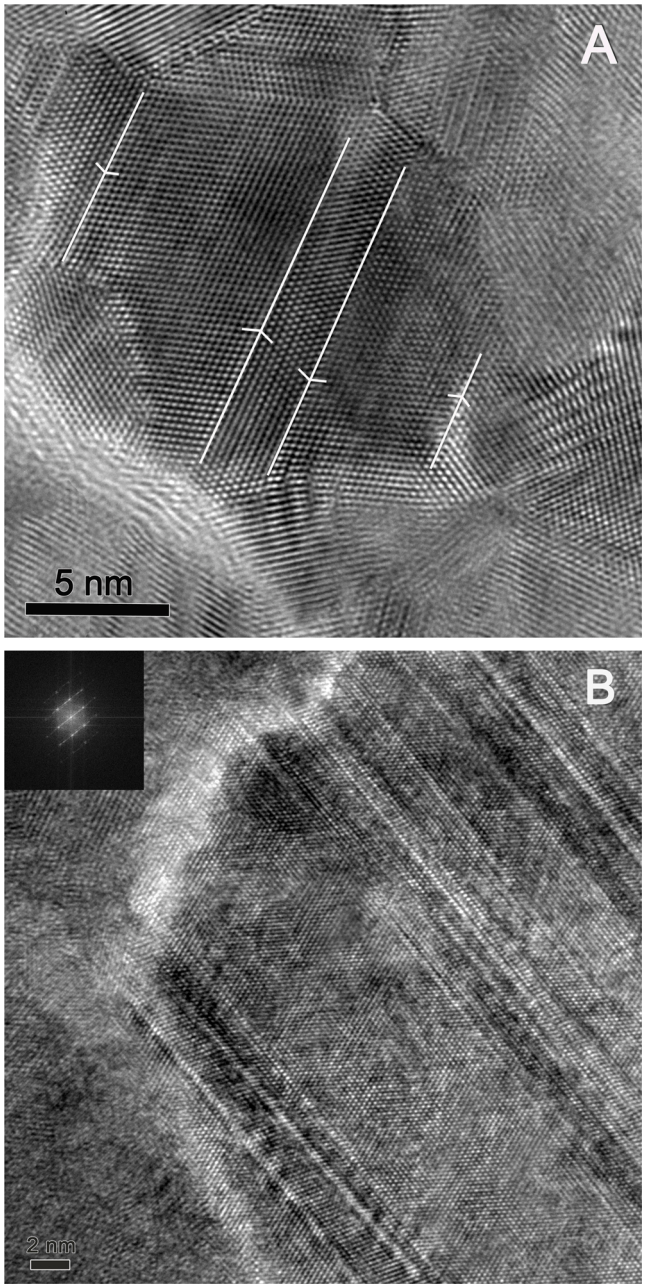

Fig. 5. High-resolution TEM images showing deformation twins identified by the mirror symmetry and parallel boundaries in (A) NC Al-2% Li and (B) NC Al. The inset in panel B is an FFT from the image.

NC Al sample achieved σ_y and σ_u of 375 MPa and 410 MPa, respectively. Grain refinement, as evidenced by the nanometric grain size of the NC Al sample (29 nm), is the main contribution behind at least ten times higher strength values obtained compared to the CG Al. On the other hand, NC Al-2% Li achieved even higher σ_y and σ_u of 440 MPa and 556 MPa, respectively, than NC Al, which is consistent with the higher average hardness values for the NC Al-2% Li compared to the NC Al discussed earlier (see Fig. 2). This extremely high strength could be attributed to the small grain size (18 nm), as shown in Figs. 3A and 4 A. In addition, solid solution strengthening due to the presence of Li could contribute to the strengthening of the NC metal through dislocation pinning [38]. Furthermore, the deformation twins observed in the small nanograins of both NC Al-2% Li and NC Al could play a role in the obtained high strength values in both samples. It is well-known that twin boundaries are barriers to dislocation motion, causing an increase in the tensile

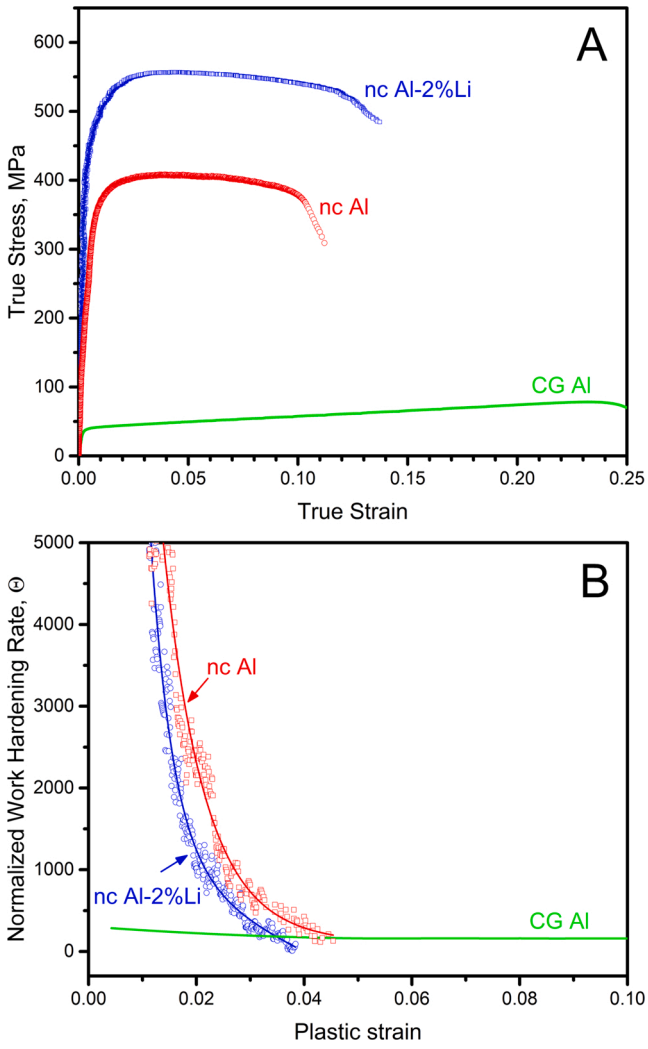

Fig. 6. (A) Tensile stress-strain curves for the NC Al-2% Li, NC Al, and the CG Al alloy. (B) The variation of the strain hardening rate as a function of the true plastic strain of the three samples.

Table 1
Tensile properties of the CG commercially pure Al and the as-milled *in-situ* consolidated NC Al-2% Li and NC Al samples.

Sample	Yield strength (MPa)	Ultimate strength (MPa)	Elastic modulus (GPa)	Uniform elongation (%)	Total elongation (%)
NC Al-Li	440 ± 11	556 ± 13	75.4 ± 1	3 ± 0.2	14 ± 1
NC Al	375 ± 13	410 ± 9	69.5 ± 1	4.5 ± 0.5	10 ± 1
CG Al	35 ± 5	80 ± 6	69.8 ± 2	23 ± 2	26 ± 3

strength of the metal. A significant improvement of tensile strength due to twinning was reported in Cu [39,40] and Ni [25]. On the other hand, Liu et al. [41] reported a comparable high ultimate tensile strength (466.7 MPa) for a spark plasma sintered and extruded ultra-fine grained (UFG) Al (188 nm). Hayes et al. [42] used ball milling in liquid N_2 followed by extrusion to synthesize UFG Al (116 nm) that exhibited a 404 MPa ultimate tensile strength. With significantly larger average grain sizes, the presence of deformation twins was not observed or reported in these UFG Al samples [41,42]. In addition, the presence of high-density second phases and dispersoids, such as nanoscale Al_2O_3 and AlN particles, was detected and was considered responsible for the majority of the strengthening in these samples rather than the inherent nanometric nature of the metal: the case in our NC Al-2% Li and NC Al *in-situ*

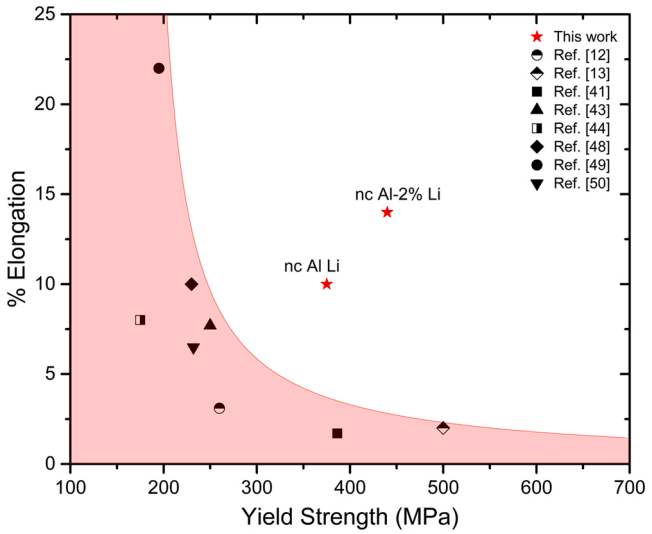

Fig. 7. The total elongation vs. the tensile yield strength of different NC and UFG Al obtained from several studies [12,13,41,43,44,48–50], and compared with the NC Al-2% Li and NC Al spheres produced in this study.

consolidated samples. Wang et al. [27] processed Al-2% Li alloys using accumulative roll bonding and aging treatment, and they were able to enhance the ultimate strength of this alloy to 353 MPa. They attributed the strength enhancement to strain hardening, grain refinement, and precipitation hardening due to the formation of Al_3Li.

Besides the extremely high strength of NC Al-2% Li and NC Al, both samples exhibit high tensile ductility, as observed from the tensile behavior in Fig. 6A. This behavior is rarely reported for NC metals and alloys with comparable grain sizes, as there exists a trade-off between strength and ductility. The high tensile yield strength of 500 MPa that was achieved in NC Al (48 nm) prepared by ball milling and hot extrusion was associated with an early plastic instability in tension, leading to failure just after yielding with total elongation of 2%, as reported by Choi et al. [13]. However, the *in-situ* consolidated NC Al-2% Li and NC Al showed significant elongation to failure: 14% and 10%, respectively. These tensile ductility values are higher than those reported for nanostructured Al samples, such as the 7.7% total elongation reported by Sun et al. [43] for a cold deformed nanostructured Al (53 nm), the 8% total elongation reported by Zakeri et al. [44] for nanostructure Al produced by ball milling followed by extrusion, and the 3.1% total elongation reported by Liu et al. [12] for nanosized Al powder pressed by SPS. Even though the different ductility behavior in these samples may have been attributed to the different deformation mechanisms specific to each sample, it has been suggested in all these reports that the limited ductility behavior originated from sample imperfections, such as pores, impurities, and cracks, which significantly affected the tensile behavior of NC samples leading to plastic failure and fracture [12,43,44].

The high tensile ductility values of NC Al-2% Li and Al in this study could reflect the integrity of their *in-situ* consolidated fully densified artifact-free nanostructures. This allowed the plastic deformation to take place without being influenced by the tensile instability or processing artifacts such as porosities or cracks that usually initiate failure in nanostructured materials [45–47]. On the other hand, good ductility has been reported for UFG Al rather than NC Al, where the enhancement in ductility is associated with larger grain sizes and thus lower strengths. Eizadjou et al. [48] used accumulative roll bonding to produce UFG Al sheets (360 nm) with a tensile yield strength of 230 MPa and good ductility of 10% elongation to failure. Khajouei-Nezhada et al. [49] reported a larger ductility of 22% elongation to failure with a 195 MPa tensile yield strength for UFG Al (410 nm) powder consolidated by high-pressure torsion. The total tensile elongation vs. yield strength are plotted in Fig. 7 to illustrate the trade off between strength and ductility for different NC and UFG Al samples fabricated using various techniques [12,13,41,43,44,48–50]. As seen in Fig. 7, most reports confirm the strength-ductility trade off as they fall in the shaded region. When comparing the results of yield strength and ductility of all the Al samples

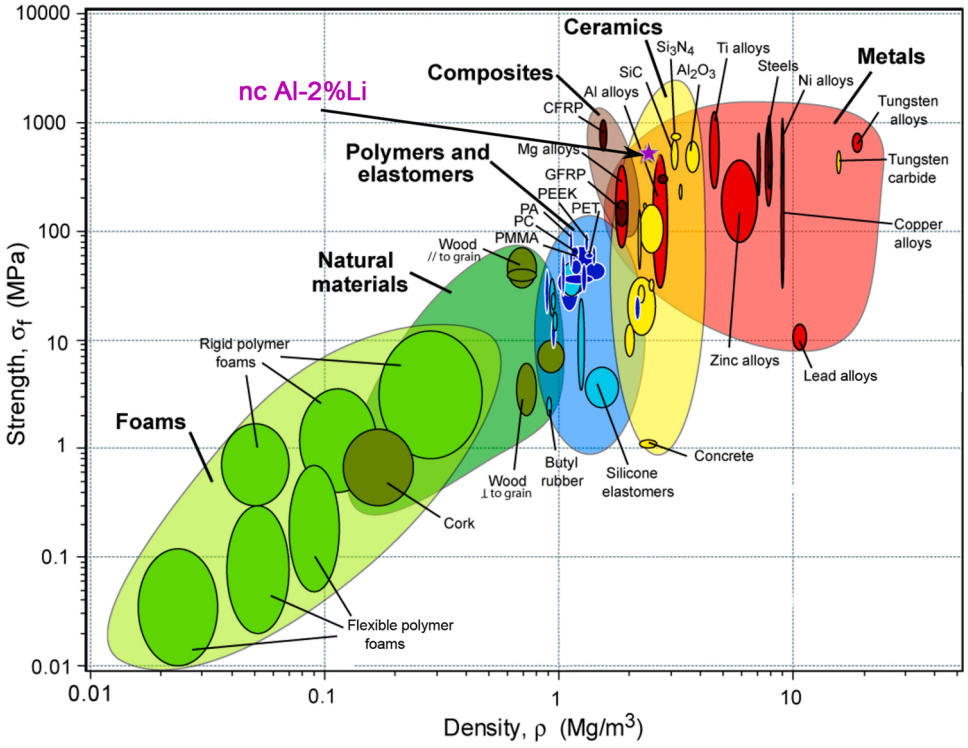

Fig. 8. The Ashby chart of yield strength (MPa) vs. density (kg/m^3). The NC Al-2% Li sample of this work is marked on the chart by the purple star. (For interpretation of the references to color in this figure legend, the reader is referred to the web version of this article.)

presented in Fig. 7, the NC Al-2% Li and NC Al samples reported in this work stand out as having achieved a good combination of high strength and good ductility. All the samples to the left of our NC Al-Li sample are reported to have comparable ductility but much lower strength than our samples. All the samples that have comparable strength to our NC Al-Li sample are reported to have much lower ductility. Thus, the NC Al-Li samples prepared in this work have the best combination of strength and ductility (440 MPa and 14%, respectively) amongst other NC and UFG Al samples.

As mentioned earlier, the interest in Al-Li alloys stems from the low weight advantage and the expected high specific strength they offer. Al is generally regarded as a low weight metal with a density of 2.7 g/cm^3. In addition, Li itself is the lightest metal with a density of 0.534 g/cm^3. It was reported that the addition of 1% Li to Al reduces the density of Al by 3% [2,3]. Thus, in our case, adding 2% Li to Al was expected to reduce the density of Al by 6%. The average density of the Al-2% Li alloy was measured and was found to be 2.54 g/cm^3, which is consistent with the 6% reduction of the Al density. Accordingly, the specific strength of the NC Al-2% Li is 0.219 MPa kg^{-1} m^{-3}. Comparing this value of specific strength to that of mild steel (0.051 MPa kg^{-1} m^{-3}) [51], this NC Al-2% Li offers a significant increase in specific strength of at least 300% over that of steel. The Ashby chart of yield strength versus density [52] is shown in Fig. 8. This chart guides the selection of materials for the best combination of lightweight and high-strength. The best strength-to-weight ratio is offered by materials located towards the upper left corner of the chart. The NC Al-2% Li sample of this work is marked on the chart by a purple star (see Fig. 8). This NC Al-2% Li sample achieved a comparable strength to steels and Ti alloys, yet at a much lower density. Furthermore, the elastic modulus of the NC Al-2% Li was calculated from the tensile data (Fig. 6a) and compared with that of the NC Al and CG Al. The average elastic modulus of the NC Al-2% Li alloy was found to be 75.4 GPa while the average elastic moduli of the NC Al and the CG Al were 69.5 GPa and 69.8 GPa, respectively. It has been reported that the addition of 1% Li to Al increases the stiffness of Al by 6% [2,3]. Thus, the increased stiffness of the NC Al-2% Li alloy can be attributed to the presence of Li.

3.3. Deformation mechanisms

The strain hardening rate is another tensile property that provides insight into the deformation mechanisms in NC materials. Fig. 6B shows the strain hardening rate, $\theta = d\sigma/d\varepsilon$, for the NC Al-2% Li, NC Al, and the commercially pure CG Al as a function of the true plastic strain. As seen in Fig. 6B, NC Al-2% Li and NC Al exhibited significantly higher θ than that of the CG Al alloy. The strain-hardening exponent values, n, of the NC Al-2% Li and NC Al were found to be 0.11 and 0.13, respectively. It has been reported that NC bulk metals with high angle grain boundaries and with grain size values less than 30 nm cannot sustain strain hardening upon loading, which leads to failure just after yielding and results in low ductility [53–56]. It was argued that as grain size decreases, small nanograins could not accommodate the repulsive interaction of strain fields of dislocations due to decreased spacing. Thus, dislocation slipping and pile-up as the dominant deformation mechanism in CG metals is essentially hindered by the grain size reduction. Nonetheless, the high θ and n of the *in-situ* consolidated NC Al-2% Li and NC Al indicate the presence of a significant dislocation activity during the tensile deformation. This observation is confirmed by a closer investigation into the nanostructure of the *in-situ* consolidated NC Al after tensile deformation, as seen in the BF-TEM image in Fig. 9A. The TEM image reveals the presence of high dislocation density distributed within the relatively

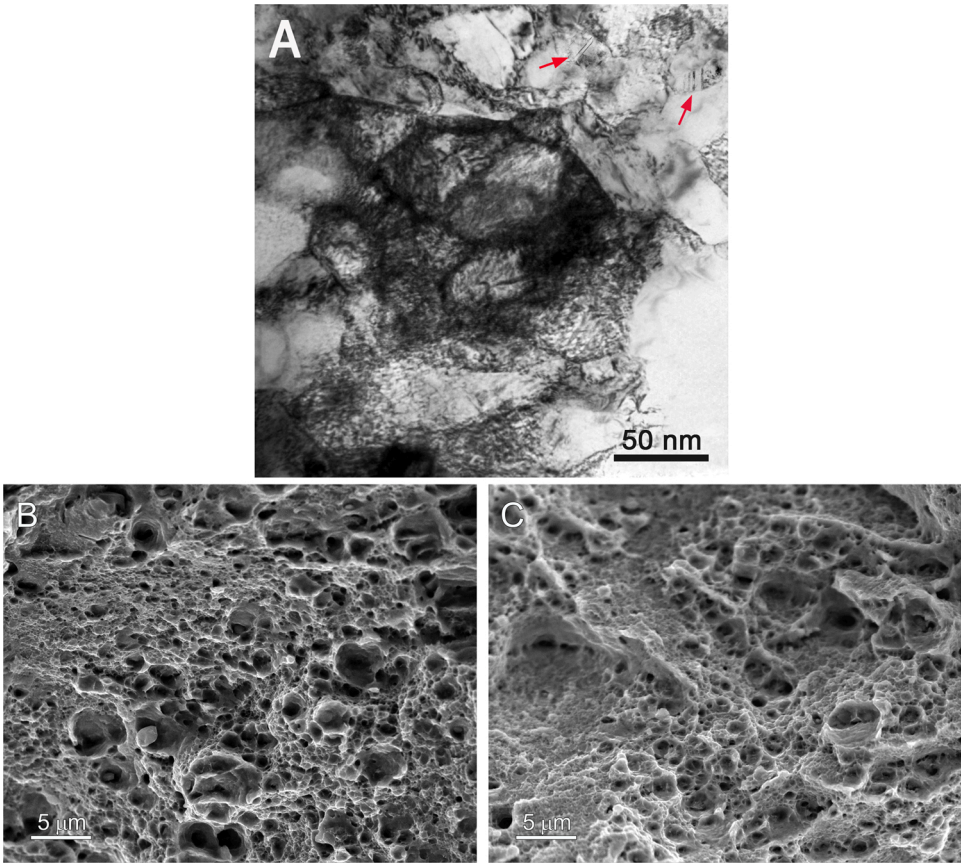

Fig. 9. (A) A bright-field TEM image of the NC Al after tensile testing showing a high density of dislocations and pile-ups in the large nanograins and deformations twins in the smaller nanograins. (B) and (C) SEM fracture surface micrographs of the NC Al and NC Al-2% Li, respectively, showing typical dimpled features that are associated with ductile plastic deformation behavior.

large grains. The large strain hardening rates of NC Al suggest that these dislocations are plastically induced during tensile testing. In addition, the fracture surface morphology presented in Fig. 9B of the NC Al sample and Fig. 9C of the NC Al-2% Li revealed the typical dimpled features associated with ductile plastic deformation behavior and dislocation activity in the nanosized grains. Furthermore, TEM investigation revealed the presence of nano twins present in the relatively smaller grains (~20 nm) (see red arrows in Fig. 9A). In light of these observations, a picture of the deformation mechanisms emerges and confirms the role and the grain size dependency of dislocations and twinning in the overall strengthening and ductility behavior of the NC Al.

Even though the NC Al-2% Li sample possesses higher elongation to failure value than that of the NC Al, the uniform elongation region where strain hardening takes place is larger in NC Al (4.5%) than in NC Al-2% Li (3%) (see Fig. 6A and Table 1). Upon applying stress above σ_y, dislocations are generated inside the grains and piled up at the grain boundaries. The smaller the grains, the faster they are saturated with dislocations, and the higher the strain hardening rate is. Thus, the increased dislocation density in the relatively larger grains of NC Al (see Fig. 9A) led to its higher uniform elongation. Accordingly, the smaller average grain size values of NC Al-2% Li (18 nm) over that of NC Al (29 nm) could plausibly explain its higher strain hardening rate and lower uniform elongation. As seen in Fig. 3, the majority of the nanograins in the NC Al-2% Li sample lie in a range similar to the preferred grain size range where twins are formed (~10−25 nm) [17,18]. This could give rise to more activated deformation twins in NC Al-2% Li than that of NC Al. As seen in Fig. 5B, several nano twins are formed into individual nanograins in the NC Al-2% Li. These results could affirm the dependency of the high strength and good ductility of the NC Al-2% Li on twinning. The higher strength and hardness of NC Al-2% Li compared to NC Al, on the other hand, are attributed to its smaller grain size, solid solution strengthening, strain hardening, and twinning.

4. Conclusion

In the present work, a combination of cryogenic and room temperature milling techniques was used to synthesize *in-situ* consolidated artifact-free bulk NC Al-2% Li alloys. This NC alloy exhibited an average grain size of 18 nm and a hardness of 1.44 GPa. The average yield and ultimate tensile strengths of the NC Al-2% Li samples was found to be as high as 440 MPa and 556 MPa, respectively. These values are higher than those of NC Al and at least 12 times higher than those of the conventional CG commercially pure Al. This extraordinarily high strength was attributed to the grain size refinement, solid solution strengthening due to the presence of Li, and the formation of deformation twins. The average uniform and total elongations of the NC Al-2% Li samples were found to be 3% and 14%, respectively. The NC Al-2% Li showed an equivalent θ to that of NC Al and higher than that of the CG Al with a strain-hardening exponent equals to 0.11. The observed strain hardening was attributed to the accumulation of dislocations during plastic deformation. The NC Al-2% Li samples achieved a comparable strength to steels and Ti alloys along with a much lower density. The TEM investigations revealed the presence of deformation twins distributed in the relatively smaller grains (10−25 nm) and emitted from the grain boundaries on {111} slip planes. The deformation twins, along with the dislocation slip and pile-ups in the relatively large grain, could be the main deformation mechanisms in the NC Al-2% and the major cause for the high θ and n values that led to good ductility. We expect that these combinations of high strength, low density, good ductility, and high strain hardening rate will have implications in the development of lightweight and tough NC Al alloys in various applications.

Credit author statement

Sara Ahmad: prepared the in-situ consolidated samples, carried out the experimental work, helped in writing the paper draft.

Leena Al-Sulaiti: analyzed data and contributed to the discussion and direction of the research.

K. Andre Mkhoyan: analyzed the TEM results and contributed to the discussion and writing of the manuscript.

Khaled Youssef: is responsible for the conceptualization of the whole study. He wrote the manuscript, validate the results, performed the nanostructure TEM analysis and the mechanical properties analysis, managed and coordinated responsibility for the research activity planning and execution.

Enclosure

C: Sara Ahmed, K. Andre Mkhoyan, and Leena Al-Sulaiti

Declaration of Competing Interest

The authors declare that they have no known competing financial interests or personal relationships that could have appeared to influence the work reported in this paper.

Acknowledgments

This work was made possible by NPRP Grant no. NPRP9-180-2-094 from the Qatar National Research Fund (a member of the Qatar Foundation). The statements made herein are solely the responsibility of the authors. The authors also acknowledge the technical support from the Central Laboratory Unit (CLU) and the Center of Advanced Materials (CAM) at Qatar University.

Appendix A. Supplementary data

Supplementary material related to this article can be found, in the online version, at doi:10.1016/j.mtcomm.2020.101607.

References

[1] J. Hirsch, Recent development in aluminum for automotive applications, Trans. Nonferrous Met. Soc. China 24 (2014) 1995.
[2] L. Zhu, N. Li, P. Childs, Light-weighting in aerospace component and system design, Propul. Power Res. 7 (2018) 103.
[3] I.J. Polmear, Aluminium alloys – a century of age hardening, Materials Forum 28 (2004) 1.
[4] K.K. Sankaran, R.S. Mishra, Aluminum alloys. Metallurgy and Design of Alloys with Hierarchical Microstructures, Elsevier, 2017, p. 57.
[5] T.H. Sanders Jr, E.S. Balmuth, Aluminum-lithium alloys: low density, Met. Prog. 113 (1978) 32.
[6] E.S. Balmuth, R. Schmidt, Aluminum-lithium alloys, in: E.A. Starke Jr., T. H. Sanders Jr. (Eds.), Proceedings of the First International CoNference on Aluminum-Lithium Alloys, Metallurgical Society of AIME, 1981, p. 69.
[7] C. Koch, D. Morris, K. Lu, A. Inoue, Ductility of nanostructured materials, MRS Bull. 24 (1999) 54.
[8] K.M. Youssef, R.O. Scattergood, K.L. Murty, C.C. Koch, Nanocrystalline Al–Mg alloy with ultrahigh strength and good ductility, Scr. Mater. 54 (2006) 251.
[9] J. Weertman, D. Farkas, K. Hemker, H. Kung, M. Mayo, R. Mitra, H. Van Swygenhoven, Structure and mechanical behavior of bulk nanocrystalline materials, MRS Bull. 24 (1999) 44.
[10] K.M. Youssef, M.A. Abaza, R.O. Scattergood, C.C. Koch, High strength, ductility, and electrical conductivity of in-situ consolidated nanocrystalline Cu-1%Nb, Mater. Sci. Eng. A 711 (2018) 350.
[11] C.C. Koch, Optimization of strength and ductility in nanocrystalline and ultrafine grained metals, Scr. Mater. 49 (2003) 657.
[12] Z.-F. Liu, Z.-H. Zhang, J.-F. Lu, A.V. Korznikov, E. Korznikova, F.-C. Wang, Effect of sintering temperature on microstructures and mechanical properties of spark plasma sintered nanocrystalline aluminum, Mater. Des. 64 (2014) 625.
[13] H. Choi, S. Lee, J. Park, D. Bae, Tensile behavior of bulk nanocrystalline aluminum synthesized by hot extrusion of ball-milled powders, Scr. Mater. 59 (2008) 1123.
[14] D. Witkin, Z. Lee, R. Rodriguez, S. Nutt, E. Lavernia, Al–Mg alloy engineered with bimodal grain size for high strength and increased ductility, Scr. Mater. 49 (2003) 297.
[15] G. Gray, J. Huang, Influence of repeated shock loading on the substructure evolution of 99.99 wt.% aluminum, Mater. Sci. Eng. A 145 (1991) 21.
[16] K.W. Jacobsen, J. Schiøtz, Nanoscale plasticity, Nat. Mater. 1 (2002) 15.
[17] V. Yamakov, D. Wolf, S.R. Phillpot, A.K. Mukherjee, H. Gleiter, Dislocation processes in the deformation of nanocrystalline aluminium by molecular-dynamics simulation, Nat. Mater. 1 (2002) 45.

[18] V. Yamakov, D. Wolf, S.R. Phillpot, H. Gleiter, Deformation twinning in nanocrystalline Al by molecular-dynamics simulation, Acta Mater. 50 (2002) 5005.
[19] B. Li, B. Cao, K. Ramesh, E. Ma, A nucleation mechanism of deformation twins in pure aluminum, Acta Mater. 57 (2009) 4500.
[20] X.Z. Liao, F. Zhou, E.J. Lavernia, D.W. He, Y.T. Zhu, Deformation twins in nanocrystalline Al, Appl. Phys. Lett. 83 (2003) 5062.
[21] X.Z. Liao, F. Zhou, E.J. Lavernia, S.G. Srinivasan, M.I. Baskes, D.W. He, Y.T. Zhu, Deformation mechanism in nanocrystalline Al: partial dislocation slip, Appl. Phys. Lett. 83 (2003) 632.
[22] M. Chen, E. Ma, K.J. Hemker, H. Sheng, Y. Wang, X. Cheng, Deformation twinning in nanocrystalline aluminum, Science. 300 (2003) 1275.
[23] J. SCHIOTZ, F. Di Tolla, K. Jacobsen, Softening of nanocrystalline metals at very small grain sizes, Nature 391 (1998).
[24] H. Van Swygenhoven, Grain boundaries and dislocations, Science 296 (2002) 66.
[25] K. Kumar, S. Suresh, M. Chisholm, J. Horton, P. Wang, Deformation of electrodeposited nanocrystalline nickel, Acta Mater. 51 (2003) 387.
[26] K.M. Youssef, R.O. Scattergood, K.L. Murty, Ultrahigh strength and high ductility of bulk nanocrystalline copper, Appl. Phys. Lett. 87 (2005), 091904.
[27] Y. Wang, H. Wu, X. Liu, J. Sun, R. Wu, L. Hou, J. Zhang, X. Li, M. Zhang, High strength ultrafine-grained Al-2Li laminate produced by accumulative roll bonding and aging processes, J. Alloy. Compd. 811 (2019), 152045.
[28] K. Rodak, A. Urbanczyk-Gucwa, M. Jabalonska, J. Pawlicki, J. Mizera, Influence of heat treatment on the formation of ultrafine-grained structure of Al-Li alloys processed by SPD, Arch. Civ. Mech. Eng. 18 (2018) 331–337.
[29] Y. Zhang, H. Ichinose, M. Nakanose, K. Ito, Y. Ishida, Transmission electron microscopic observation of grain boundaries in CVD diamond thin films, J. Electron Microsc. 45 (1996) 436.
[30] E. Botcharova, J. Freudenberger, L. Schultz, Mechanical and electrical properties of mechanically alloyed nanocrystalline Cu–Nb alloys, Acta Mater. 54 (2006) 3333.
[31] C. Suryanarayana, Mechanical alloying and milling, Prog. Mater. Sci. 46 (2001) 1.
[32] F. Zhao, L. Wang, D. Fan, B.X. Bie, X.M. Zhou, T. Suo, Y.L. Li, M.W. Chen, C.L. Liu, M.L. Qi, M.H. Zhu, S.N. Luo, Macrodeformation twins in single-crystal aluminum, Phys. Rev. Lett. 116 (2016), 075501.
[33] Y. Zhu, X. Liao, S. Srinivasan, Y. Zhao, M. Baskes, F. Zhou, E. Lavernia, Nucleation and growth of deformation twins in nanocrystalline aluminum, Appl. Phys. Lett. 85 (2004) 5049.
[34] M. Muzyk, Z. Pakiel, K. Kurzydlowski, Generalized stacking fault energies of aluminum alloys–Density functional theory calculations, Metals 8 (2018) 823.
[35] J. Venables, Deformation twinning in face-centered cubic metals, Philos. Mag. 6 (1961) 379–396.
[36] R. Asaro, P. Krysl, B. Kad, Deformation mechanism transitions in nanoscale FCC metals, Philos. Mag. Lett. 83 (2003) 733–743.
[37] H. Rösner, J. Markmann, J. Weissmüller, Deformation twinning in nanocrystalline Pd, Philos. Mag. Lett. 84 (2004) 321–334.
[38] R. Scattergood, C.C. Koch, K. Murty, D. Brenner, Strengthening mechanisms in nanocrystalline alloys, Mater. Sci. Eng. A 493 (2008) 3.
[39] L. Lu, Y. Shen, X. Chen, L. Qian, K. Lu, Ultrahigh strength and high electrical conductivity in copper, Science 304 (2004) 422.
[40] K. Lu, L. Lu, S. Suresh, Strengthening materials by engineering coherent internal boundaries at the nanoscale, Science 324 (2009) 349.
[41] J. Liu, C. Liang, Microstructure characterization and mechanical properties of bulk nanocrystalline aluminium prepared by SPS and followed by high-temperature extruded techniques, Mater. Lett. 206 (2017) 95.
[42] R. Hayes, D. Witkin, F. Zhou, E. Lavernia, Deformation and activation volumes of cryomilled ultrafine-grained aluminum, Acta Mater. 52 (2004) 4259.
[43] X.K. Sun, H.T. Cong, M. Sun, M.C. Yang, Preparation and mechanical properties of highly densified nanocrystalline Al, Metall. Mater. Trans. A 31 (2000) 1017.
[44] M. Zakeri, A. Vakili-Ahrarirudi, Effect of milling speed and shaping method on mechanical properties of nanostructure bulked aluminum, Mater. Des. 37 (2012) 487.
[45] C.C. Koch, Proc. J. Metastable Nanocryst. Mater. (2003) unpublished.
[46] E. Ma, Instabilities and ductility of nanocrystalline and ultrafine-grained metals, Scr. Mater. 49 (2003) 663.
[47] M.A. Meyers, A. Mishra, D.J. Benson, Mechanical properties of nanocrystalline materials, Prog. Mater. Sci. 51 (2006) 427.
[48] M. Eizadjou, H.D. Manesh, K. Janghorban, Microstructure and mechanical properties of ultra-fine grains (UFGs) aluminum strips produced by ARB process, J. Alloy. Compd. 474 (2009) 406.
[49] M. Khajouei-Nezhad, M.H. Paydar, R. Ebrahimi, P. Jenei, P. Nagy, J. Gubicza, Microstructure and mechanical properties of ultrafine-grained aluminum consolidated by high-pressure torsion, Mater. Sci. Eng. A 682 (2017) 501.
[50] A.M. Esawi, N.T. Aboulkhair, Bi-modally structured pure aluminum for enhanced strength and ductility, Mater. Des. 83 (2015) 493.
[51] S. Abdullah, S. Beden, A.K. Ariffin, Z.M. Nopiah, A. Zaharim, P.D.M.M. Rahman, in: Fatigue Life Assessment of a Shell Structure from Different Steel Types: a Case Study Using variable Amplitude Loadings. In: The World Scientific and Engineering Academy and Society, Organizer, Proceedings of the 8th Conference on Simulation, Modelling, and Optimization, 2008, pp. 153–159.
[52] M. Ashby, Materials Selection in Mechanical Design, fourth ed., Butterworth-Heinemann- an imprint of Elsevier, Oxford, 2011.
[53] D. Jia, K. Ramesh, E. Ma, Failure mode and dynamic behavior of nanophase iron under compression, Scr. Mater. 42 (1999) 73.
[54] D. Jia, Y. Wang, K. Ramesh, E. Ma, Y. Zhu, R. Valiev, Deformation behavior and plastic instabilities of ultrafine-grained titanium, Appl. Phys. Lett. 79 (2001) 611.
[55] T. Malow, C. Koch, P. Miraglia, K. Murty, Compressive mechanical behavior of nanocrystalline Fe investigated with an automated ball indentation technique, Mater. Sci. Eng. A 252 (1998) 36.
[56] G.T. Gray, T.C. Lowe, C.M. Cady, R.Z. Valiev, I.V. Aleksandrov, Influence of strain rate & temperature on the mechanical response of ultrafine-grained Cu, Ni, and Al-4Cu-0.5Zr, Nanostruct. Mater. 9 (1997) 477.